# Optimization of Virtual Monoenergetic Image Generation Using Photon-Counting CT: Evaluation of Material Decomposition Approaches with Phantom Data

Hebah Al Said, Abderaouf Behouch, Mohammed Alzaabi, Aamir Raja, Nabil Maalej
College of Engineering and Physical Sciences, Department of Physics, Khalifa University, Abu Dhabi, UAE

2026 JULY 19–22 VANCOUVER, BC
JOINT AAPM | COMP MEETING

## ABSTRACT

In this study, we optimized the virtual monoenergetic image (VMI) using a single-photon counting computed tomography (SPCCT). A QRM phantom containing tissue-equivalent and contrast-agent inserts was scanned using a five-bin SPCCT acquisition protocol. Two-material and three-basis material decomposition were investigated to identify optimal energy-bin and basis-material combinations for VMI generation. Image quality was evaluated using objective metrics of CNR, SNR, and clinicians' scores. The most effective decomposition strategy was validated using an ex vivo beef tissue to assess its applicability to realistic biological tissue.

The results demonstrated that optimized VMIs can enhance image quality, especially in low contrast at high resolution and texture. Although three-material decomposition provided additional flexibility, the two-material approach showed robust and consistent performance for both phantom and biological tissue studies. The findings highlight the potential of optimized SPCCT VMI generation to improve tissue differentiation and support enhanced diagnostic CT imaging.

## CONTACT

Nabil Maalej
Khalifa University
Abu Dhabi, UAE
nabil.maalej@ku.ac.ae
00971-566470084

## INTRODUCTION

Spectral photon-counting computed tomography (SPCCT) enables energy-resolved imaging and the generation of virtual monoenergetic images (VMIs), which can improve tissue contrast, reduce artifacts, and enhance image quality. In this study, we conducted a comprehensive comparison of all possible energy-bin and basis-material combinations to optimize VMI generation in SPCCT using a multi-material phantom and ex-vivo tissue phantom.

## METHODS AND MATERIALS

A QRM multi-material phantom (Fig. 1) containing water, adipose, muscle, hydroxyapatite (HA100 and HA200), and iodine inserts (10 and 15 mg/mL) was scanned using a spectral photon-counting CT (SPCCT) (MARS scanner) (Fig. 2) with a five energy bins: bin 1 (7-40 KeV), bin 2 (40-50 KeV), bin 3 (50-60 KeV), bin 4 (60-79 KeV), and bin 5 (80-118 KeV). Calibration curves were established by relating the experimentally measured average linear attenuation coefficients (LACs) to those derived from the NIST database. The SPCCT images were used for virtual monoenergetic image (VMI) reconstruction. VMIs were reconstructed for 10–100 keV in 10 keV steps using two- and three-material decompositions and all possible combinations of basis materials and SPCCT energy bins. Image quality was assessed using contrast-to-noise ratio (CNR), signal-to-noise ratio (SNR), relative error (RE) in linear attenuation coefficient (LAC), and clinician scores (CS).
Using Material decomposition, we can assume that LAC at each pixel is a linear combination of basis materials. In the two-material case:

$$\mu(E) = A\mu_1(E) + B\mu_2(E)$$

Where $\mu(E)$ is the measured LAC at energy $E$, $\mu_1(E)$ and $\mu_2(E)$ are the LACs of the two basis materials at the same energy, and $A$ and $B$ are the weighting coefficients for each material. This formalism was extended to three materials and three energy bins. Two clinicians independently scored image quality on a 10-point scale, and the final CS was the average of their assessments. Optimal VMI parameters were selected based on the highest CNR and CS across all combinations. Validation was performed on an ex vivo beef phantom containing muscle, fat, bone, and iodine inserts using the same SPCCT protocol, and image quality metrics were evaluated.

**Figure 1.** QRM materials phantom (QRM GmbH, Germany).

**Figure 2.** MARS Bioimaging SPCCT Scanner.

| Basis Materials | Energy Bins | VMI energies with RE < 5% | VMI optimal energy (keV) | CS | CNR | SNR | RE (%) |
|---|---|---|---|---|---|---|---|
| I15 and Water | 2,4 | 40-100 | 40 | **9.5** | 1.56 | 6.45 | 0.66 |
| HA200 and Water | 2,4 | 40-80 | 40 | 8.5 | **1.59** | 6.34 | 1.63 |
| HA200 and Water | 2,5 | 40-70 | 40 | 9 | 1.54 | 6.09 | 1.53 |

**Table 1.** Optimal VMIs from two-basis material decomposition. The highest clinician score (CS) image and the highest CNR image are reported, considering only VMIs with RE < 5%.

## RESULTS

For each energy bin, a linear relationship was observed between the experimentally measured average linear attenuation coefficients (LACs) and the LACs calculated using the NIST data. The highest CNR among all VMIs was achieved at 40 keV using a three-basis-material decomposition (iodine (15 mg/mL), adipose-equivalent material, and water). However, the highest clinician scores for image quality were obtained at 40 keV using both two basis materials decomposition (iodine (15 mg/ml) and water) (Fig. 3(a), Fig 4, Table 1) and three basis materials decomposition (iodine (15 mg/ml), hydroxyapatite (200 mg/ml), and water) (Fig. 3(b), Table 2). Validation with an ex vivo biological tissue phantom (Fig. 5 and 6 ) confirmed the optimal VMIs generation.

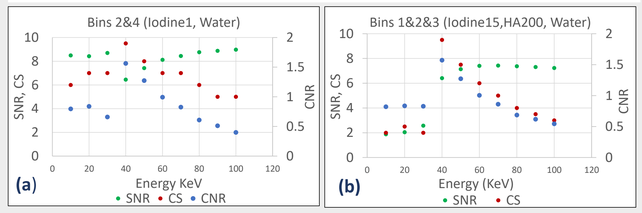


**Figure 3:** CNR, SNR, and clinician score (CS) metrics for VMIs produced using (a) two- and (b) three-material decompositions.

| Basis Materials | Energy Bins | VMI energies with RE < 5% | VMI optimal energy (keV) | CS | CNR | SNR | RE (%) |
|---|---|---|---|---|---|---|---|
| I15 and HA200 and Water | 1,2,3 | 40-100 | 40 | **9.5** | 1.57 | 6.41 | 1.95 |
| I15 and Adipose and Water | 2,4,5 | 40-100 | 50 | 7 | 1.53 | 10.36 | 0.39 |
| I15 and Adipose and Water | 2,4,5 | 40-100 | 40 | 6 | **1.77** | 7.96 | 0.44 |
| I15 and Muscle and Water | 2,4,5 | 50-80 | 50 | 9 | 1.48 | 9.23 | 0.51 |
| HA200 and Adipose and Water | 2,3,5 | 40-100 | 50 | 6.5 | 1.43 | 9.69 | 2.88 |
| HA200 and Adipose and Water | 2,3,5 | 40-100 | 40 | 6 | 1.67 | 7.63 | 3.66 |
| HA200 and Muscle and Water | 2,3,4 | 50-100 | 50 | 7 | 1.28 | 6.83 | 0.40 |

**Table 2.** Optimal VMIs from three-basis material decomposition. The highest clinician score (CS) image and the highest CNR image are reported, considering only VMIs with RE < 5%.

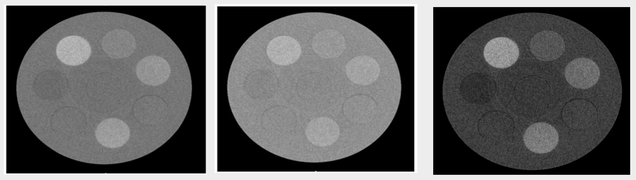

**(a)** SPCCT image for energy bin2 **(b)** SPCCT image for energy bin 4 **(c)** Optimal VMI at 40 keV

**Figure 4:** Two basis material optimal VMI obtained using Iodine (15 mg/ml) and solid water basis materials, and for energy bins 2 (a) and 4 (b). (c) shows the optimal VMI at 40 keV, selected based on best clinician scoring (CS = 9.5).

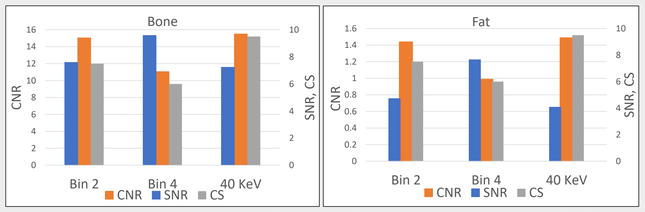


**Figure 5:** Bar charts showing CNR (left y-axis), SNR, and clinician score (CS) (right y-axis) for bone and fat tissues with muscle tissue used as background, for SPCCT images for energy bins 2 and 4, and the VMI at 40 keV.

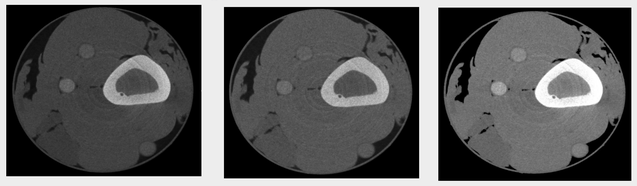

**(a)** SPCCT image for energy bin 2 (40-50 keV) **(b)** SPCCT image for energy bin 4 (60-79 keV) **(c)** VMI at 40 keV

**Figure 6:** Comparison of the 40 keV VMI with the SPCCT images from energy bins 2 and 4 for the ex vivo biological tissues phantom with iodine inserts.

## DISCUSSION

From Table 1, it can be observed that, for the two-basis material decomposition, the highest clinician score (CS = 9.5) was achieved for the 40 keV VMI using iodine (15 mg/ml) and water as the basis materials and using images from energy bins 2 and 4. For the three-basis material decomposition (Table 2), the highest clinician score (CS = 9.5) was obtained for the 40 keV VMI using iodine (15mg/ml), HA (200 mg/ml), and water as basis materials and energy bins 1, 2, and 3 images. Quantitative image quality metrics do not necessarily align with clinician preferences: Table 1 and Table 2 show that some VMIs achieved higher CNR values but lower clinician scores.
The VMI generation for the biological tissue phantom (Figure 5) shows that the VMI image outperforms the original SPCCT images. The bone tissue exhibits the highest contrast in the 40 keV VMI, with a CNR of 15.5, compared to CNR of 15.0 and 11.0 for the energy bins 2 and 4 images, respectively. The fat tissue shows low overall contrast, with a slightly higher CNR in the 40 keV VMI (1.49) compared to the SPCCT images at energy bins 2 (1.44) and 4 (0.99), reflecting a modest improvement in fat-muscle differentiation. The SNR varies with energy, and bin 4 shows the highest SNR for both bone (9.58) and fat (7.65). The measured attenuation coefficients for bone and fat in the 40 keV VMI were in good agreement with the NIST reference values, with relative errors of 6.85% and 5.78%, respectively, confirming the accuracy of the linear attenuation coefficients in the VMIs. These results indicate that the phantom-optimized parameters translate well to biological tissue imaging, enhancing the clinician's score for both fat and bone tissues.

## CONCLUSIONS

We have demonstrated through this study the optimization of VMI generation and quality. We compared two- and three-basis material decomposition for all possible energy combinations of the SPCCT scanner. The results demonstrate that the selection of basis materials and the optimization of energy-bin combinations significantly affect VMI quality. The optimized parameters were also applicable to a biological tissue phantom. Although quantitative metrics, such as CNR and SNR, are widely used image quality metrics, clinician scoring plays a crucial role in determining diagnostically optimal images. Combining both quantitative and qualitative image quality scores provides a robust and comprehensive VMI optimization framework.

## REFERENCES

1. R. E. Alvarez, A. Macovski, Energy-selective reconstructions in x-ray computerized tomography, Physics in Medicine & Biology 21 (5) (1976) 733.
2. J. Wang, X. Duan, C. H. McCollough, Material decomposition and post-processing: History and basic principles, in: Spectral Imaging: Dual-Energy, Multi-Energy and Photon-Counting CT, Springer, 2022, pp. 3–14.
3. L. Ren, C. H. McCollough, L. Yu, Three-material decomposition in multi-energy CT: impact of prior information on noise and bias, SPIE-Intl Soc Optical Eng, 2018, p. 51. doi:10.1117/12.2294953.

© Poster Template by Genigraphics® 1.800.790.4001 www.genigraphics.com